Common nonmutational *NOTCH1* activation in chronic lymphocytic leukemia

Giulia Fabbri[a], Antony B. Holmes[a], Mara Viganotti[a], Claudio Scuoppo[a], Laura Belver[a], Daniel Herranz[a], Xiao-Jie Yan[b], Yasmine Kieso[b], Davide Rossi[c,d], Gianluca Gaidano[e], Nicholas Chiorazzi[b], Adolfo A. Ferrando[a,f,g], and Riccardo Dalla-Favera[a,f,h,i,1]

[a]Institute for Cancer Genetics and the Herbert Irving Comprehensive Cancer Center, Columbia University, New York, NY 10032; [b]The Feinstein Institute for Medical Research, Northwell Health, Manhasset, New York, NY 11030; [c]Division of Hematology, Oncology Institute of Southern Switzerland, 6500 Bellinzona, Switzerland; [d]Lymphoma and Genomics Research Program, Institute of Oncology Research, 6500 Bellinzona, Switzerland; [e]Division of Haematology, Department of Translational Medicine, Università del Piemonte Orientale, 28100 Novara, Italy; [f]Department of Pathology and Cell Biology, Columbia University, New York, NY 10032; [g]Department of Pediatrics, Columbia University, New York, NY 10032; [h]Department of Genetics & Development, Columbia University, New York, NY 10032; and [i]Department of Microbiology & Immunology, Columbia University, New York, NY 10032

Contributed by Riccardo Dalla-Favera, February 15, 2017 (sent for review December 20, 2016; reviewed by Carlo M. Croce and Louis M. Staudt)

Activating mutations of *NOTCH1* (a well-known oncogene in T-cell acute lymphoblastic leukemia) are present in ∼4–13% of chronic lymphocytic leukemia (CLL) cases, where they are associated with disease progression and chemorefractoriness. However, the specific role of *NOTCH1* in leukemogenesis remains to be established. Here, we report that the active intracellular portion of NOTCH1 (ICN1) is detectable in ∼50% of peripheral blood CLL cases lacking gene mutations. We identify a "NOTCH1 gene-expression signature" in CLL cells, and show that this signature is significantly enriched in primary CLL cases expressing ICN1, independent of *NOTCH1* mutation. NOTCH1 target genes include key regulators of B-cell proliferation, survival, and signal transduction. In particular, we show that NOTCH1 transactivates *MYC* via binding to B-cell–specific regulatory elements, thus implicating this oncogene in CLL development. These results significantly extend the role of *NOTCH1* in CLL pathogenesis, and have direct implications for specific therapeutic targeting.

chronic lymphocytic leukemia | NOTCH1 | transcriptional network

Chronic lymphocytic leukemia (CLL) is a common hematologic tumor characterized by the clonal expansion of $CD5^+$ B cells (1, 2). Recent investigations have provided a comprehensive picture of the CLL genome, revealing its relatively low burden of genetic lesions, with a small number of frequently mutated "driver" genes. CLL mutated genes include the *NOTCH1* oncogene, the splicing regulator *SF3B1*, the tumor-suppressors *TP53* and *ATM*, and several B-cell receptor (BCR)/NF-κB regulators, such as *MYD88*, *BIRC3*, and *NFKBIE*, among others (3–7).

NOTCH1, a well-known oncogene in T-cell acute lymphoblastic leukemia (T-ALL) (8, 9), has emerged as the most commonly mutated gene in CLL at diagnosis, accounting for ∼4–13% of patients (3–7). *NOTCH1* encodes a transmembrane receptor that, upon binding to a ligand expressed on the surface of a "signal-sending" cell, undergoes a series of conformational changes and proteolytic cleavages, ultimately allowing the translocation of its intracellular, cleaved, and active portion (hereinafter referred to as "ICN1") to the nucleus (10, 11). Once in the nucleus, ICN1 binds to the DNA-binding protein RBPJ, the main effector of NOTCH-signaling, and recruits a series of coactivator proteins to induce transcriptional activation of target genes (10, 11). NOTCH1 target genes mediate regulation of fundamental biological processes, such as development, cell differentiation, cell-fate decision, proliferation, and apoptosis (10, 11).

In contrast to T-ALL, where the majority of mutations are represented by constitutively activated ligand-independent alleles affecting the heterodimerization domain of the protein, most *NOTCH1* mutational events in CLL are represented by PEST [proline (P), glutamic acid (E), serine (S), threonine (T)-rich protein sequence] -truncations removing the phosphodegron sequence required for FBXW7-mediated ICN1 proteasomal degradation; in a minority of cases, point mutations in the 3′UTR of the *NOTCH1* mRNA lead to aberrant splicing events that also remove the PEST domain of the NOTCH1 protein (3–7). *NOTCH1* mutations in CLL were shown to associate with poor prognosis, including a specific subset of patients carrying trisomy 12, disease progression, transformation to highly aggressive diffuse large B-cell lymphomas, termed Richter syndrome, and immunochemotherapy resistance (3, 4, 12–16).

Despite this potentially relevant role in the CLL clinical course, the oncogenic role of *NOTCH1* in this disease remains poorly understood. Although few NOTCH1 targets have been shown to be overexpressed in *NOTCH1*-mutated cases compared with wild-type CLL (4, 17, 18), the full spectrum of genes controlled by NOTCH1 and their contribution to the disease pathogenesis have not been identified. Moreover, recent reports documented that CLL cells in the lymph node frequently express ICN1, independent of *NOTCH1* PEST-truncation (19, 20), especially within the proliferation centers, which represent the key microanatomical sites of interaction of CLL cells with accessory cells and proliferation (21). Accordingly, these findings have been interpreted as the result of microenvironmental signals activating the NOTCH1 cascade. Conversely, the status of *NOTCH1*

Significance

A pathogenetic role of *NOTCH1* in chronic lymphocytic leukemia (CLL) has been implied by the presence of deregulating mutations in a relatively small fraction of cases. Our results now indicate that ∼50% of CLL cases devoid of mutations express the active form of NOTCH1 ICN1 (intracellular portion of NOTCH1), thus implicating a much broader role of this transcription factor in the disease. $ICN1^+$ CLL cases display equivalent NOTCH1-dependent transcriptional responses regardless of the gene mutation status, indicating that the detection of ICN1 represents a reliable biomarker of *NOTCH1* activation for diagnostic and therapeutic targeting. Finally, our results identify the NOTCH1-dependent transcriptional program in CLL cells, thus providing direct insights into the pathogenesis of a large fraction of CLL cases.

Author contributions: G.F., A.A.F., and R.D.-F. designed research; G.F., M.V., C.S., L.B., and D.H. performed research; A.B.H., X.-J.Y., Y.K., D.R., G.G., and N.C. contributed new reagents/analytic tools; X.-J.Y., Y.K., D.R., G.G., and N.C. provided subject samples; G.F., A.A.F., and R.D.-F. analyzed data; and G.F. and R.D.-F. wrote the paper.

Reviewers: C.M.C., The Ohio State University; and L.M.S., National Cancer Institute, National Institutes of Health.

The authors declare no conflict of interest.

Data deposition: The data reported in this paper have been deposited in the Gene Expression Omnibus (GEO) database, www.ncbi.nlm.nih.gov/geo [accession nos. GSE12195 (GeneChip Human Genome U133 Plus 2.0, Affymetrix; expression data from normal mature B-cell subsets), GSE92626 (RNA-Seq data), and GSE92701 (ChIP-Seq data)].

[1]To whom correspondence should be addressed. Email: rd10@columbia.edu.

This article contains supporting information online at www.pnas.org/lookup/suppl/doi:10.1073/pnas.1702564114/-/DCSupplemental.

activation in the peripheral blood (PB) compartment of CLL patients is less clear (4, 7, 18, 22).

To address these questions, we have analyzed the functional status of ICN1 in normal mature B cells and in a panel of PB CLL cells including both *NOTCH1*-mutated and wild-type cases. We report broader *NOTCH1* activation, significantly extending beyond the mutated cases and the transcriptional consequences of this activation in leukemic B cells.

Results

***NOTCH1* Is Activated in Naïve and Memory B Cells, the Putative Normal Counterparts of CLL.** To obtain a comparative baseline before investigating the activity of *NOTCH1* in CLL, we first defined the expression and activation pattern of *NOTCH1* in normal mature B-cell subsets. We performed gene-expression profiling as well as ICN1 immunoblot analysis in naïve, germinal center (GC) and memory B cells isolated from human tonsils (23). Although the phenotype of the B cell expanding to generate overt CLL remains a matter of debate, naïve and memory B cells are considered the most likely putative normal counterparts of this disease (24–26). The levels of *NOTCH1* mRNA and of the cleaved and active intracellular portion of NOTCH1 ICN1 were abundant in naïve and memory B cells, whereas they were almost undetectable in GC B cells (Fig. 1 *A* and *B*). Immunofluorescence staining of human tonsillar biopsies confirmed these findings, revealing ICN1 nuclear staining in the B-cell fraction populating the mantle zone of the GCs, which is highly enriched in naïve B cells (Fig. 1*C* and Fig. S1).

Gene set enrichment analysis (GSEA) using the "Hallmark_Notch_Signaling" signature from the Molecular Signature Database (27) confirmed that ICN1 expression in naïve and memory B cells is associated with NOTCH1 transcriptional activity (Fig. 1*D*). Taken together, these data indicate that *NOTCH1* is physiologically expressed and activated in the cells of origin of CLL.

PB CLL Cells Express ICN1 in both *NOTCH1*-Mutated and Wild-Type Cases. We next investigated the incidence of NOTCH1 pathway activation in CLL by analyzing peripheral blood CLL cells (>70% purity in 90 of 93 cases analyzed by cytofluorimetry analysis for $CD5^+/CD19^+$) (*Materials and Methods*) from a cohort of primary CLL cases (n = 124). Twenty-two percent of these cases carried *NOTCH1* PEST-truncating events (n = 27 of 124) (Dataset S1), representative of the prototypical p.P2515fs mutation (n = 17 of 29, 58.6%), frameshift deletions (n = 3 of 29, 10.3%), and nonsense mutations (n = 5 of 29, 17.2%). In addition, four cases carried 3′UTR *NOTCH1* mutations known to lead to aberrant splicing events disrupting the PEST domain of the ICN1 protein (7). The majority of *NOTCH1*-mutated CLL cases carried unmutated *IGHV* genes (n = 23 of 24 with known *IGHV* status, 95.8%), as previously reported (3, 4, 12).

Notably, ICN1 was detectable by immunoblot analysis in 50.5% (n = 49 of 97) of *NOTCH1*–wild-type cases (Fig. 2 *A* and *B* and Fig. S2*A*). Among these, ICN1 expression occurred in 53.3% (n = 24 of 45) of *IGHV* mutated and 41.9% (n = 13 of 31) of *IGHV*-unmutated cases, respectively (Dataset S1).

As expected, all *NOTCH1* PEST-disrupted CLL cases expressed a truncated active form of the protein (Fig. 2 *A* and *B* and Fig. S2*A*) (4, 7). The levels of ICN1 expression were variable across the panel, with *NOTCH1*-mutated cases often displaying higher levels of ICN1 compared with wild-type samples (Fig. S2*A*). ICN1 levels in *NOTCH1*–wild-type cases were responsive to NOTCH inhibition by the γ-secretase inhibitor Compound-E (28) (Fig. S2*B*).

Immunofluorescence analysis showed that strong nuclear ICN1 expression was detectable in virtually 100% of CLL cells in both *NOTCH1*-mutated and wild-type $ICN1^+$ CLL cases (Fig. 2*C*). Moreover, ICN1 was not expressed in PB mononuclear cells (PBMCs) from healthy, age-matched elderly individuals (Fig. S2*C*). These observations exclude the possibility that ICN1 expression in *NOTCH1*–wild-type cases was because of residual contamination by normal cells. Altogether, these results suggest that the activation of the *NOTCH1* oncogene in CLL is more common than what is currently known based on the frequency of *NOTCH1* activating mutations (*Discussion*).

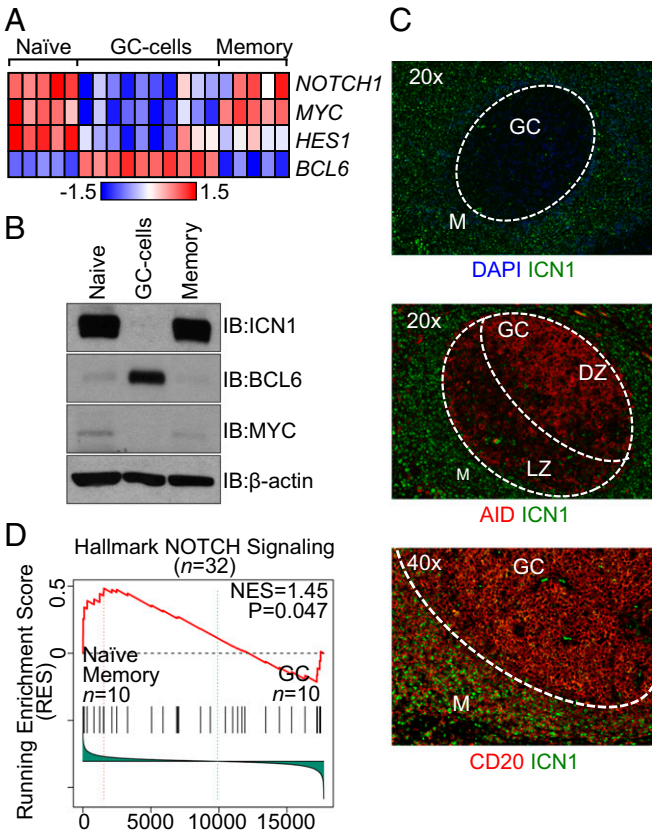

Fig. 1. *NOTCH1* is expressed and activated in naïve and memory B cells, putative normal counterparts of CLL. (*A*) Gene-expression profile analysis (HG-U133 Plus 2.0 Array) of *NOTCH1*, *MYC*, *HES1*, and *BCL6* in normal mature naive, GC, and memory B-cell subpopulations isolated from human tonsils (23). Each column corresponds to an independent sample. The mRNA expression pattern of *NOTCH1* in naïve and memory B cells is similar to that of *MYC*, typically expressed only in a small fraction of GC–B cells (69), and opposite to that of *BCL6*, a known GC master regulator (81). Moreover, *NOTCH1* expression levels are concordant with those of *HES1*, a NOTCH1 target in multiple tissue types (11). (*B*) Immunoblot (IB) analysis of ICN1, BCL6, MYC, and control β-actin in mature B-cell subpopulations isolated from human tonsils. (*C*) Immunofluorescence (IF) staining of ICN1, the dark-zone GC-marker AID (82), and the B-cell–specific surface antigen CD20 in a human tonsil section. (*D*) Tracking of the HALLMARK_NOTCH_SIGNALING geneset from the Molecular Signatures Database v5.1 (software.broadinstitute.org/gsea/msigdb/index.jsp) in normal mature B-cell subpopulations by GSEA. Abbreviations: DZ, dark zone; LZ, light zone; M, mantle zone.

Identification of the CLL NOTCH1-Direct Transcriptional Program. As a tool to further interrogate the functional activity of *NOTCH1* in $ICN1^+$ CLL cells and to shed light on the NOTCH1-controlled biological functions in CLL, we next investigated the NOTCH1-dependent CLL transcriptional program. We used a CLL cell line (MO1043) (29), which carries a hemizygous *NOTCH1* PEST-truncation and expresses a truncated ICN1 that is responsive to NOTCH inhibition by the γ-secretase inhibitor Compound-E (28). Given the low intrinsic signaling activity of PEST-truncated alleles alone (8) (Fig. S3*A*), we sought to investigate NOTCH1-dependent programs using an inducible lentiviral system expressing either an HA-tagged constitutively active form of NOTCH1 (ICN1-HA) or control eGFP upon doxycycline addition (Fig. S3*B*) (30). Induction of NOTCH1 signaling was demonstrated by HA immunoblot and

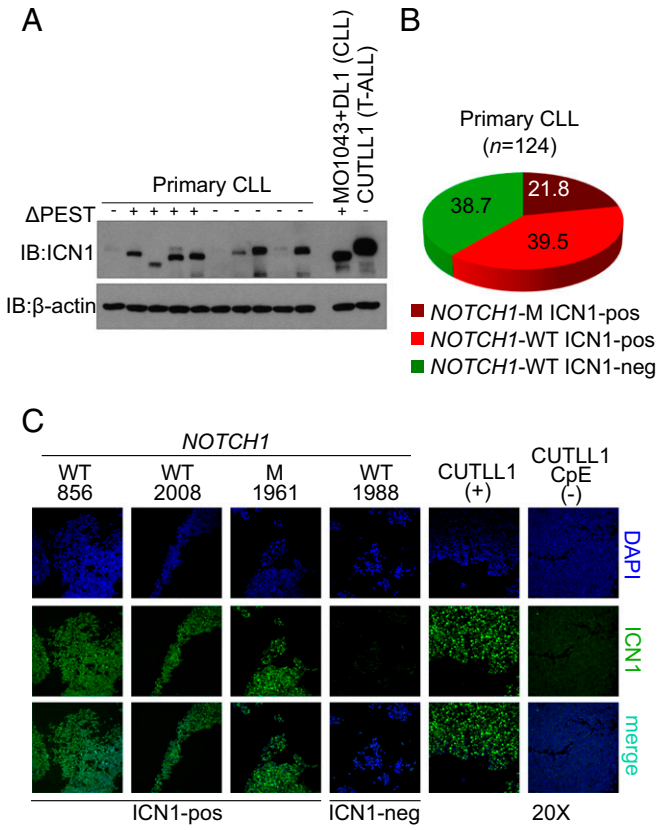

Fig. 2. Primary CLL cases express ICN1 because of *NOTCH1* PEST-truncations or alternative mechanisms. (*A*) IB analysis of ICN1 and control β-actin in 10 representative PB CLL cases, 4 carrying *NOTCH1* PEST-truncations (ΔPEST) and 6 *NOTCH1*–wild-type (WT), in the control T-ALL cell line CUTLL1 (83) and in MO1043 CLL cells cocultured with OP9 stromal cells expressing the NOTCH1 ligand DL1 (54). The full set of analyzed primary CLL cases, including those reported here, is displayed in Fig. S2. (*B*) Frequency of ICN1 positivity in 124 primary CLL cases. (*C*) IF staining of ICN1 in primary ICN1^{+} (pos) and ICN1^{-} (neg) CLL cells and in the control CUTLL1 T-ALL cell line in basal conditions (+) and upon Compound E (CpE, 24 h, 1 μM) treatment (–).

quantitative RT-PCR (qRT-PCR) for *DTX1*, a well-established NOTCH1-direct target gene (11) (Fig. S3 *C–E*). This experimental system was used to identify genetic elements bound and directly regulated by NOTCH1 by integrating RNA-Seq and NOTCH1 ChIP-Seq data (Datasets S1–S3).

Unsupervised clustering of RNA-Seq data showed that the expression profiles of MO1043-ICN1-HA and -eGFP cells cluster separately (Fig. 3*A*). Supervised analysis revealed that ICN1-HA induction leads to up-regulation of over 700 transcripts [false-discovery rate (FDR) < 0.001, median fold-change 1.7, range = 1.1–170.4], including known NOTCH1 targets, such as HES/HEY family members, *NRARP*, *DTX1*, and *NOTCH1* itself, as expected (Fig. 3*B*), as well as genes involved in immune and signaling pathways relevant for the development and activation of B cells (Datasets S4 and S5).

ChIP-Seq analysis identified a total of 4,737 NOTCH1 binding sites, mapping to promoters in ∼40% of the cases, and to intragenic or distal regulatory regions of the genome in ∼60% of the cases (Fig. 3 *C* and *D*). The integration of NOTCH1 ChIP-Seq profiles with those of the H3K4me3, H3K4me, H3K27Ac, and H3K27me3 histone modifications (Fig. S4) revealed that ∼94% of NOTCH1 proximal binding sites displayed chromatin marks characteristic of active promoters, whereas ∼37% of the distal ones were associated with putative active enhancers (Fig. 3*E*) (31–33). Analysis of H3K27Ac patterns across the genome identified 917 superenhancers (34), many of which involved genes defining key functions of B cells and displayed sequence motif enrichment of transcription factors known to be master regulators of B-cell identity (Fig. 3*F*, Fig. S5 *A* and *B*, and Datasets S6 and S7) (35–38). NOTCH1-binding at super-enhancer regions (n = 698 of 4,737 binding sites, 14.7%) was prominently involved in the activation of genes implicated in B-cell differentiation and activation and antiapoptotic functions (Fig. 3 *G* and *H* and see below).

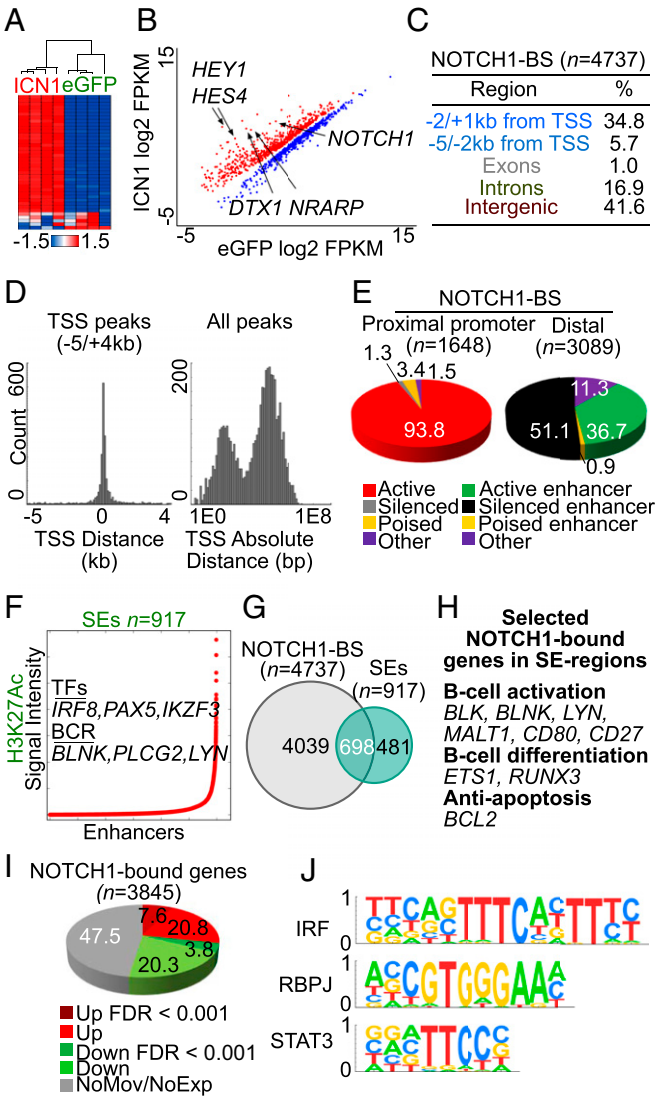

Fig. 3. Identification of NOTCH1 direct targets in CLL. (*A*) Hierarchical clustering of RNA-Seq profiles of MO1043-ICN1-HA and -eGFP cells (Pearson correlation with average linkage, minimum $\log_2$ expression 5 and minimum SD 1). (*B*) Scatter plot of $\log_2$-transformed RNA-Seq FPKM values of differentially expressed genes between MO1043-ICN1-HA and -eGFP control CLL cells (FDR < 0.001). (*C* and *D*) Distribution of NOTCH1 binding sites (BS) in the genome of MO1043-ICN1-HA CLL cells. (*E*) Functional classification of NOTCH1-BS mapping to proximal promoters and distal regions of the genome based on their overlap with the H3K4me3, H3K4me, H3K27Ac and H3K27me3 histone marks. (*F*) Rank order of increasing H3K27Ac fold-enrichment at enhancer loci in in MO1043-ICN1-HA CLL cells. (*G*) Overlap between NOTCH1-BS and superenhancers identified with the ROSE algorithm (35, 36). (*H*) Representative examples of genes regulated by NOTCH1 via binding to superenhancer regions. (*I*) Intersection between RNA-Seq and ChIP-Seq data obtained in MO1043-ICN1-HA CLL cells. (*J*) Top three significantly (P = 1.00E-15) enriched transcription factor motifs lying ±200 bp of NOTCH1-BS. Abbreviations: NoExp, transcripts not expressed in MO1043-ICN1-HA cells; NoMov, transcripts not moving upon ICN1-HA expression; SEs, superenhancers; TF, transcription factor.

The intersection between the genes differentially expressed upon ICN1-HA induction as identified by RNA-Seq and the NOTCH1 binding profiles obtained through ChIP-Seq revealed a significant overlap between the two sets ($P < 0.001$), with ~39% of genes induced by ICN1-HA (FDR < 0.001) being bound by NOTCH1 (Fig. 3*I* and Fig. S6). Notably, genes associated with NOTCH1 binding sites in superenhancer regions were more often up-regulated upon ICN1-HA induction compared with those associated with NOTCH1 binding sites in other genomic regions (52% vs. 29%, $P < 0.001$) (Fig. S5*C*). Motif enrichment analysis of sequences surrounding the NOTCH1 binding sites (±200 bp) and associated with significant (FDR < 0.001) up-regulation of the corresponding genes ($n = 503$) confirmed significant ($P = 1.00E-15$) enrichment of the DNA motifs of RBPJ, the main effector of NOTCH signaling (11), as well as of binding sequences of other potential cooperating cofactors, including NF-κB, PU.1, ETS, and STAT family members (Fig. 3*J* and Dataset S8).

The NOTCH1-Dependent CLL Signature Is Detectable in *NOTCH1*–Wild-Type CLL Cases Expressing ICN1. To identify bona fide direct NOTCH1 targets to be used as a tool to interrogate primary CLL cells (NOTCH1 CLL signature), we selected genes bound by NOTCH1 and the transcripts of which were up-regulated by ICN1-HA with a FDR < 0.001. Two-hundred and ninety-one

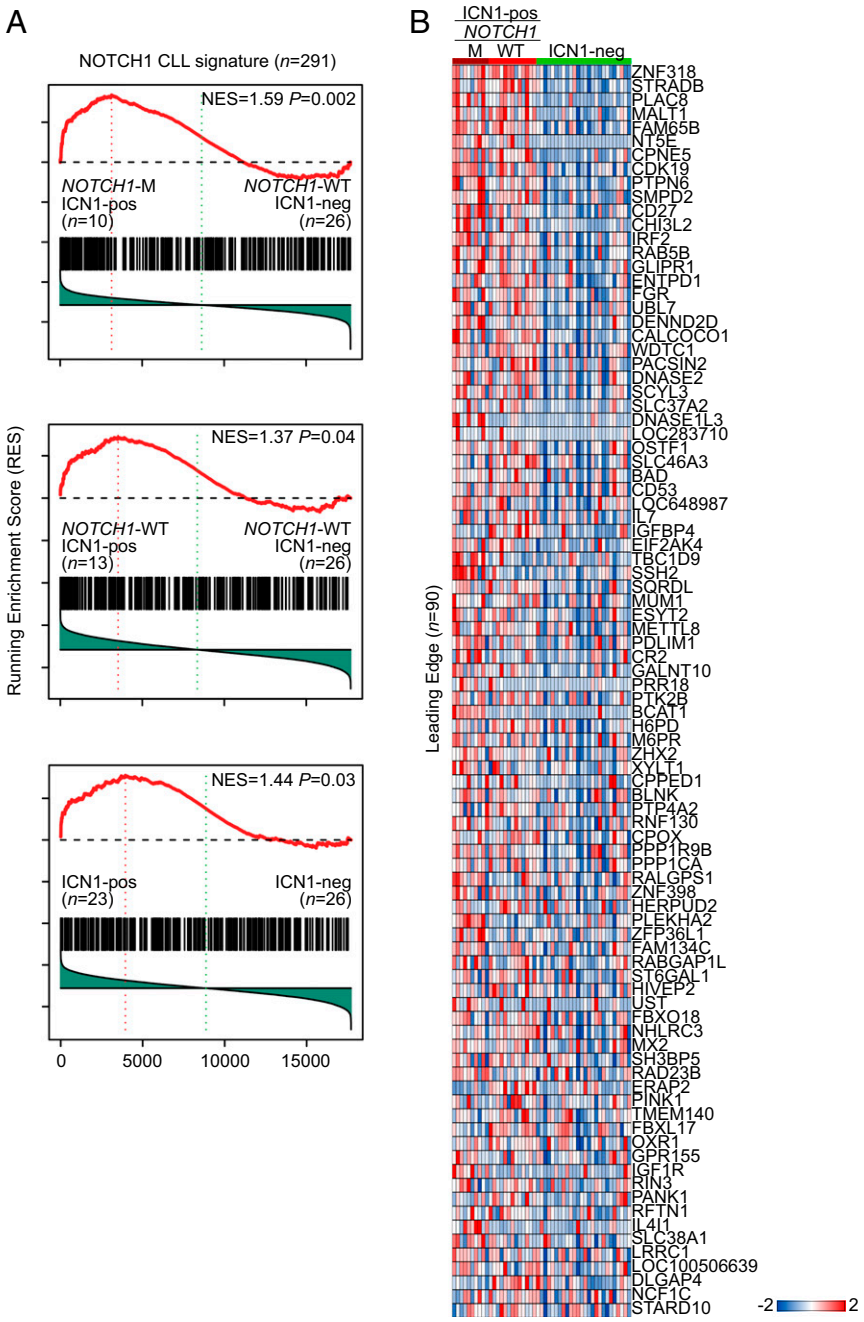

Fig. 4. The NOTCH1 CLL signature is enriched in primary CLL cases expressing ICN1. (*A*) GSEA enrichment plots depicting significant enrichment of the NOTCH1 CLL signature in *NOTCH1*-mutated (M) and wild-type (WT) primary CLL cases expressing ICN1$^+$ (ICN1-pos) compared with ICN1$^-$ (ICN1-neg) cases, and heatmap of RNA-Seq profiles of corresponding leading edge genes ($n = 90$) (*B*).

genes met these criteria, including NOTCH1 target genes, such as *HES1*, *DTX1*, *JAG1*, and *NOTCH1* itself, among others, as well as NF-κB, antiapoptotic, and cytokine-chemokine genes (Dataset S9).

To determine whether *NOTCH1*–wild-type ICN1$^+$ CLL cases display evidence of NOTCH1 signaling activation analogous to *NOTCH1*-mutated cases, we explored the presence of the NOTCH1 CLL signature identified above in RNA-Seq data from 49 PB CLL samples fully characterized in terms of *NOTCH1* mutation and ICN1 protein expression. This panel included 10 *NOTCH1*-mutated cases expressing ICN1 (including three cases carrying *NOTCH1* 3′UTR events), 13 *NOTCH1*–wild-type cases expressing ICN1, and 26 cases devoid of both *NOTCH1* mutations and ICN1 expression (Fig. S2*A*). GSEA analysis (27) revealed significant enrichment of the NOTCH1 CLL signature both in *NOTCH1*-mutated ($P = 0.002$) and *NOTCH1*–wild-type ($P = 0.04$) cases expressing ICN1 compared with ICN1$^-$ cases (Fig. 4*A*). Leading edge genes ($n = 90$) determining a significant ($P = 0.03$) enrichment of the NOTCH1 CLL signature in ICN1$^+$ cases were overall expressed at similar levels in *NOTCH1*-mutated and wild-type ICN1$^+$ cases [average fragments per kilobase of transcript per million mapped reads (FPKM) 54.3 and 51.3, respectively], with few genes expressed at higher levels in the *NOTCH1*-mutated ones ($n = 9$ of 90, $P < 0.05$) (Fig. 4*B* and Dataset S10).

Thus, ICN1 is also functionally active in ICN1$^+$ CLL cases devoid of *NOTCH1* mutations, indicating that they are functionally equivalent in terms of NOTCH1-dependent transcriptional responses to *NOTCH1*-mutated ones (*Discussion*).

***NOTCH1* Regulates Genes with Key Functions in B-Cell Physiology.** Functional annotation of the full set of genes bound (ChIP-Seq) and dynamically connected (RNA-Seq) to NOTCH1 revealed that NOTCH1 directly regulates general functions involved in cell proliferation and survival (Datasets S11 and S12). The former included *CCND3*, which encodes a cyclin necessary for G1/G2 transition (39) via direct binding to the gene promoter, consistent with a previous report in T-ALL (40). Among the latter, *BCL2* and *MCL1*, two antiapoptotic genes with a well-established role in the pathogenesis of CLL, emerged as novel targets of NOTCH1, likely regulated through long-range dynamic interactions (24, 41–43).

The NOTCH1 transcriptional program included also a cadre of genes with specific functions in B-cell physiology (Fig. S7). Among these are BCR signaling pathway genes, including upstream pathway members (e.g., *LYN*, *SYK*, *BLK*, *BLNK*, *CR2*, and *PIK3CD*), as well as downstream effectors, such as MAPK (e.g., *MAP3K1*, *KRAS*, and *RRAS*) and NF-κB cascade members (e.g., *IKBKB*, *NFKB1*, and the CBM signalosome complex member *MALT1*) (44). NOTCH1 also appears to activate the NF-κB target *NFKBIA*, which encodes the NF-κB repressor IκBα (44), and *PTPN6*, encoding SHP-1, an important negative modulator of antigen-receptor signaling in lymphocytes (45), suggesting a role of NOTCH1 in a delayed negative-feedback of activation of this cascade (46). *CXCR4*, which encodes a chemokine receptor relevant for the chemotaxis of CLL cells toward microenvironmental cells expressing the CXCL12 ligand (47), emerged as a novel NOTCH1 target in CLL. This axis is fundamental for the exit of CLL cells from lymph nodes and, accordingly, the expression of the CXCR4 receptor has been shown to associate with a higher risk of lymphoid organ infiltration and poor disease outcome (48). Finally, among several NOTCH-pathway related genes, NOTCH1 induced the expression of *JAG1*, which encodes for a ligand of NOTCH1 reported to be expressed on the surface of CLL cells (22), suggesting a positive feed-forward loop in signaling activation.

NOTCH1 Transactivates *MYC* in CLL. *MYC* is a central oncogene in human malignancy, an established *NOTCH1* target in T-ALL and is involved in CLL progression (3, 13, 49–51). Thus, we investigated the relationship between *NOTCH1* activation and *MYC* gene expression in CLL. Consistent with previous reports (52), we observed two putative superenhancers located ∼500 kb upstream of the *MYC* oncogene both in MO1043-ICN1-HA cells and primary CLL cases (Fig. 5 *A* and *B*). These superenhancers were also present in CD19$^+$ and CD20$^+$ B cells, small lymphocytic lymphoma, and mantle cell lymphoma (52), but not in the majority of ∼90 distinct tissue types (37), suggesting context specificity (Fig. 5*C* and Fig. S8*A*). NOTCH1 ChIP-Seq analysis of MO1043-ICN1-HA cells revealed the presence of multiple NOTCH1 peaks and RBPJK conserved motifs in this region. Specifically, one superenhancer within region 8q24 (chr8:128191039–128239723, hg19) contained one NOTCH1 binding site and two RBPJK motifs, whereas a second one (chr8:128299403–128321023, hg19), contained four NOTCH1 binding sites and three RBPJK motifs (Fig. 5*B*). Local ChIP analysis of NOTCH1 and the H3K27Ac mark in MO1043-ICN1-HA cells confirmed NOTCH1 binding at these epigenetically active superenhancers (Fig. 5*D*).

Intriguingly, our meta-analysis of copy number (CN) data obtained in two independent collections of CLL patients (7, 53) revealed that this region is recurrently affected by duplications in CLL ($n = 15$ of 452 and $n = 15$ of 353), including focal ones specifically encompassing this superenhancer cluster (Fig. 5*A* and Fig. S8 *B* and *C*), suggesting that these genetic lesions may affect *MYC* expression in CLL. Moreover, we observed that *NOTCH1* mutations and *MYC* locus duplications, including those focally affecting only this superenhancer region, were largely mutually exclusive in primary CLL patients (7) (Fig. S8*D*), similarly to CLL cells that have undergone Richter syndrome transformation (3, 13).

To demonstrate a direct functional relationship between *NOTCH1* and *MYC* in CLL, we first investigated whether *NOTCH1* activation could promote *MYC* transcription in ICN1$^-$ or ICN1-low primary CLL cells cocultured with stromal cells expressing the NOTCH1 ligand Delta-1 (OP9-DL1) (54). CLL cells cocultured with OP9-DL1 cells showed an increased level of *MYC* RNA, which was specifically dependent upon NOTCH1 expression because it was abrogated in the presence of the NOTCH-inhibitor Compound E (Fig. 5*E* and Fig. S9). Reciprocally, NOTCH1 inhibition by Compound E induced *MYC* down-regulation in ICN1-positive CLL cases (Fig. 5*E* and Fig. S9). These results indicate that *NOTCH1* controls *MYC* expression in ICN1$^+$ CLL cells.

Discussion

CLL cells in the lymph node are known to display frequent *NOTCH1* activation independent of mutation, as documented by their frequent immunohistochemical positivity for ICN1 in lymph node sections of both *NOTCH1*-mutated and wild-type cases (19, 20). Conversely, few reports have shown activation of *NOTCH1* in PB CLL samples, and the results involved a relatively low number of cases and a possibly low sensitivity of detection, leading to a significant underestimation of the ICN1$^+$ cases (4, 7, 18, 22). Our finding that ∼50% of PB CLL cases lacking *NOTCH1* mutations express ICN1 strongly suggests that the activation of this pathway is more common than what is predicted by the frequency of classic *NOTCH1* PEST-truncations. These findings have implications for the mechanisms leading to *NOTCH1* activation in normal and transformed cells, for the understanding of the pathogenesis of CLL, and the development of anti-NOTCH1 targeted therapies.

Mechanisms of *NOTCH1* Activation in PB CLL Cells. The common detection of ICN1 in the nucleus of CLL cells within lymph nodes in both *NOTCH1*-mutated and wild-type cases has been interpreted as an induction by microenvironmental interactions with cells expressing NOTCH1 ligands (19, 20). Conversely, the frequent detection of ICN1 in *NOTCH1*–wild-type PB CLL cells shown herein raises the issue, shared also by *NOTCH1*-mutated cases carrying activation-dependent alleles, of the mechanisms leading to signaling induction. Although it is plausible that CLL cells may continuously recirculate between the PB and secondary niches, such as the lymph

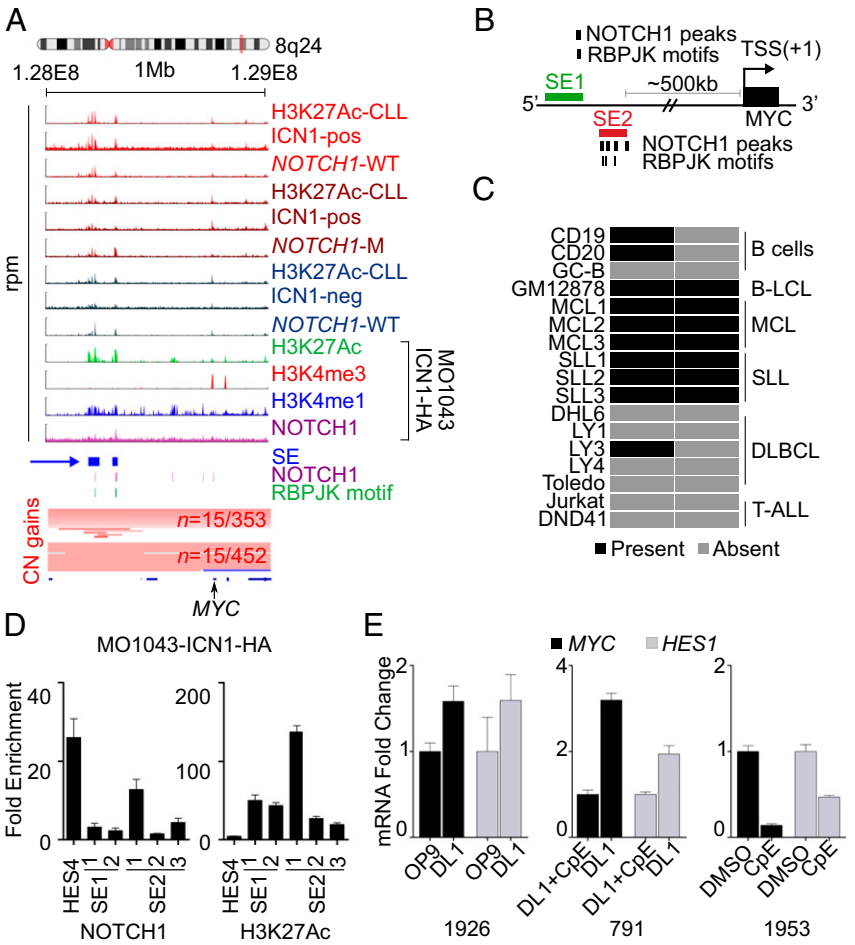

Fig. 5. A NOTCH1-bound superenhancer region regulating *MYC* expression is recurrently duplicated in CLL. (*A*) NOTCH1 occupancy profiles and histone marks patterns in the 8q24 region encompassing the *MYC* locus (chr8:128000000–129000000, hg19) in primary CLL cases and MO1043-ICN1-HA cells, with corresponding peaks depicted in the box below the ChIP-Seq plots. The *y* axes in the ChIP-Seq plots indicate fragment density in reads per million (rpm). The two boxes below the called peaks represent segmentation data (7, 53) visualized using IGV (2.3.59), with red denoting a region of CN gain, blue a CN loss, and white depicting a normal (diploid) CN. Individual genes in the region are aligned in the *Bottom* panel. (*B*) Schematic representation of the distribution of superenhancers, NOTCH1 binding sites, and RBPJ motifs in the 8q24 region encompassing the *MYC* locus. (*C*) In the heatmap, rows correspond to normal or malignant B cells (52, 84) and two control T-ALL cell lines, and columns represent the two superenhancers identified in the 8q24 region encompassing the *MYC* locus, color-coded based on their presence or absence in the displayed cell type (light gray, absent; black, present). (*D*) ChIP-qPCR analysis of NOTCH1 and H3K27Ac at the *MYC*-associated superenhancer regions identified in MO1043-ICN1-HA CLL cells; results are presented relative to those obtained with IgG (IgG; control) and to a distal actin locus, set as 1. (*E*) qRT-PCR analysis of *MYC* and *HES1* mRNA expression in three representative primary CLL cases, upon NOTCH1 signaling induction via coculture on stromal OP9-DL1 cells in the presence or absence of the γ-secretase inhibitor Compound E (CpE, 24 h, 1 μM, *Left* and *Center*), or upon basal NOTCH1 signaling inhibition in the presence of CpE (*Right*). Results are represented relative to those of CLL cells cocultured on OP9 stromal cells (*Left*), on OP9-DL1 stromal cells in the presence of CpE (*Center*), or with vehicle DMSO (*Right*), set as 1. The full set of analyzed primary CLL cases, including those represented here, is displayed in Fig. S9. The bar graphs in *D* and *E* show the mean values, and the error bars represent the SD between triplicates. Abbreviations: B-LCL, B-lymphoblastoid cell line; DLBCL, diffuse large B-cell lymphoma; MCL, mantle cell lymphoma; SE, superenhancer; SLL, small lymphocytic lymphoma.

nodes, thus being exposed to signals triggering NOTCH1 activation, several observations seem to disfavor the possibility that the ICN1 presence observed in these cells is because of residual signaling form the nodal environment. It has been shown that perinodal CLL cells rapidly lose nuclear ICN1 expression once they move beyond the lymph node capsule (19). The half-life of ICN1 is short and variable, from less than an hour to a few hours in several tested cell types (55), including primary CLL cells, but it is significantly shorter than the long life of CLL cells in the PB, which has been estimated to be of at least several days (56). These observations, together with the fact that ICN1 is expressed in virtually all CLL cells in ICN1$^+$ cases (Fig. 2*C*), are consistent with the continuous induction of the NOTCH1 cascade in CLL cells in the blood stream. However, future studies should compare ICN1 levels in the peripheral blood and in the nodal CLL compartment of the same individual to achieve a better understanding of the dynamics of ICN1 expression in different anatomic compartments within the same CLL patient.

It is conceivable that sustained *NOTCH1* activation in the PB may be mediated by cell-autonomous and ligand-dependent mechanisms. Among the former, activation of alternative cryptic *NOTCH1* promoters has been reported in human and, more frequently, murine T-ALL (57–59). However, this mechanism was preliminarily excluded by the analysis of H3K27Ac ChIP-Seq data in a panel of nine CLL cases, all of which displayed high levels of the H3K27Ac mark decorating only the canonical 5′ transcriptional start site (TSS) of the *NOTCH1* gene (Fig. S10). Additional ligand-independent mechanisms include activation by other signaling pathways, as reported for the T-cell receptor pathway in T cells (60), or aberrant vesicle trafficking of the NOTCH1 receptor (61). Ligand-dependent mechanisms include binding to ligands expressed by endothelial cells in the blood vessels or by the CLL cells themselves (18, 22).

Role of *NOTCH1* in B-Cell Development and CLL Pathogenesis. Our results indicate that *NOTCH1* displays a stage-specific expression pattern in mature B cells, being expressed and activated in naïve and memory B cells, which are considered the cells of origin of CLL (1). The enrichment of our NOTCH1 CLL signature in these normal subpopulations compared with GC B cells suggests that the biological programs orchestrated by *NOTCH1* in CLL are similar to those already active in the putative normal B-cell counterparts of the disease. Thus, the finding of *NOTCH1* activation in CLL cells reflects the constitutive, dysregulated expression of a physiologic signal and its corresponding gene-expression program rather than an ectopic program associated with transformation. The set of *NOTCH1*-direct transcriptional target genes suggests a broad program aimed at promoting the survival and proliferation of mature B cells by supporting BCR and cytokine signaling and their downstream effectors, such as PI3K and NF-κB pathways. NOTCH1 direct targets specifically relevant for the B-cell phenotype appear to be regulated via direct activation of the corresponding promoters, as well as via long-range interactions occurring at superenhancer sites, consistent with the role of these large regulatory elements in orchestrating the expression of cell-type specific genes (37).

Role of NOTCH1-Induced *MYC* Expression. An important component of the NOTCH1-controlled program in CLL cells is the transactivation of the *MYC* oncogene. Our data suggest that this transactivation is mediated by the binding of NOTCH1 to B-cell–specific superenhancers located ∼500 kb upstream of the *MYC* locus. This region interacts with the *MYC* promoter in small lymphocytic lymphoma and mantle cell lymphoma, and also leads to *MYC* transcriptional activation in Epstein–Barr-transformed lymphoblastoid cells as a result of Epstein–Barr virus nuclear antigen 2 binding (52, 62). The focal recurrent duplications of this locus observed in CLL (7, 53), analogous to what is observed in other malignancies in which CN gains affect the tissue-specific enhancers involved in *MYC* expression (50, 63, 64), suggest that the gain of context-specific superenhancers represents a common mechanism for up-regulating *MYC* expression in distinct tumor types. However, the detection of this superenhancer cluster also in CLL cases devoid of ICN1 expression (Fig. 5*A*), and the observation that *MYC* mRNA levels were not significantly different between $ICN1^+$ and $ICN1^-$ CLL cases indicate that other transcription factors are likely involved in the regulation of this locus in B cells, as previously suggested for EBF and RELA in Epstein–Barr-transformed lymphoblastoid cells (62).

Clinical Implications. The observation that the NOTCH1 CLL signature is enriched in $ICN1^+$ CLL cases independent of *NOTCH1* mutation significantly increases the fraction of CLL cases that may be dependent on constitutive NOTCH1 activity. *NOTCH1* mutations are known to associate with adverse CLL clinical and biological features, including an unmutated *IGHV* status (12), and predict a poor outcome when found in CLL patients at diagnosis (12). Conversely, our results showed that ICN1 expression in cases devoid of *NOTCH1* mutations occurred at similar frequencies in *IGHV*-mutated and *IGHV*-unmutated CLL cases. However, the relatively small and heterogeneous cohort of patients analyzed in this study did not provide us with the statistical power of establishing reliable correlations between ICN1 expression and the clinical course of the disease. Thus, dedicated prospective clinical studies are warranted to assess the biological and prognostic associations of ICN1 expression rather than *NOTCH1* mutations in CLL alone, especially in the context of anti-CD20–based therapies. This analysis may allow further refinement of the recent mutation/cytogenetic hierarchical model of classification of patients with CLL in distinct risk classes (65). Finally, we propose that ICN1 expression may also represent a more reliable biomarker of *NOTCH1* activation in the testing of prognostic criteria and therapeutics agents targeting NOTCH1 (28, 66).

Materials and Methods

Cell Lines and Isolation of Human B-Cell Subsets. MO1043 cells (29) were cultured in Iscove's Modified Dulbecco's Medium (Life Technologies) supplemented with 20% (vol/vol) FBS (Sigma-Aldrich), penicillin (100 U/mL), and streptomycin (100 μg/mL). The identity of the cell line was verified by CN analysis using the Genome-Wide Human SNP Array 6.0 (Affymetrix), as previously reported (3). HEK 293T cells were cultured in Dulbecco's Modified Eagle Medium (Life Technologies) with 10% (vol/vol) FBS, 100 U/mL penicillin, and 100 μg/mL streptomycin. OP9 and OP9-DL1 cells were grown in Minimum Essential Medium Alpha Medium (Corning) supplemented with 20% (vol/vol) FBS, 100 U/mL penicillin, 100 μg/mL streptomycin, and 2 mM glutamine (Thermo Fisher Scientific) (54). Human GC B cells, naive B cells, and memory B cells were isolated from reactive tonsils as described previously (23). Compound E was obtained from Enzo Life Sciences and used at a final concentration of 500 nM to 1 μM in DMSO vehicle.

Protein Extraction and Immunoblot Analysis. Whole-cell extracts were obtained using Nonidet P-40 lysis buffer (150 mM NaCl, 1.5% (vol/vol) Nonidet P-40, 50 mM Tris·HCl pH 8.0, 2 mM EDTA pH 8.0) supplemented with proteinase inhibitor mixture (Sigma-Aldrich), according to a previously described protocol (67). Protein lysates were resolved on 4–12% Tris-Glycine gels (Novex, Life Technologies). Subcellular fractionation was performed as previously described (68). Samples were incubated with primary antibodies overnight at 4 °C. The following primary antibodies were used: rabbit monoclonal anticleaved NOTCH1 (clone D3B8, Cell Signaling Technology), mouse monoclonal anti-MYC (clone 9E10, Santa Cruz), mouse monoclonal anti-BCL6 (clone GI191E/A8, Cell Marque), rabbit monoclonal anti-HA (clone C29F4, Cell Signaling Technology), mouse monoclonal anti–β-actin (clone AC-15, Sigma), rabbit polyclonal anti–β-tubulin (H-235, Santa Cruz). Horseradish peroxidase-conjugated secondary antibodies and ECL or West Dura reagent (Thermo Fisher Scientific) were used for signal detection.

Immunofluorescence Analysis. Immunofluorescence analysis of ICN1, AID, and CD20 was performed on formalin-fixed paraffin-embedded material from human tonsils and primary peripheral blood CLL cells according to standard procedures using the following antibodies: rabbit monoclonal anticleaved NOTCH1 (clone D3B8, Cell Signaling Technology), rat monoclonal anti-AID (clone mAID-2, eBioscience), and mouse monoclonal anti-C20 (clone L26, Thermo Fisher) (69).

ChIP. MO1043-ICN1-HA cells (cells induced to express ICN1-HA with 1 μg/mL of doxycycline for 36 h) were cross-linked with 1% formaldehyde for 10 min at room temperature, quenched by the addition of glycine to a final concentration of 0.125 M and frozen at –80 °C. Cross-linked chromatin was fragmented by sonication with the Bioruptor sonicator (Diagenode) to achieve fragment sizes of ∼200–500 bp using the following sonication buffer: 10 mM Tris·HCl pH 8.0, 100 mM NaCl, 1 mM EDTA pH 8.0, 0.5 mM EGTA pH 8.0, 0.1% Na-Deoxycholate, and 0.5% *N*-lauroylsarcosine. Sheared chromatin was incubated overnight with 10 μL of NOTCH1 antisera (70), 4 μg of antibodies to H3K27Ac (Active Motif, cat#39133) or H3K4me3 (Abcam, cat#ab8580), or 2 μg of antibodies to H3K4me1 (Abcam, cat#ab8895) or H3K27me3 (Active Motif, cat#39157) (ENCODE Project: genome.ucsc.edu/ENCODE/antibodies.html). Protein A magnetic beads were added for 4 h at 4 °C, followed by sequential washes at increasing stringency and reverse cross-linking. After RNase and proteinase K treatment, ChIP DNA was purified using the MiniElute Reaction Clean Up Kit (Qiagen) and quantified by Quant-iT PicoGreen dsDNA Reagent (Life Technologies). Validation via quantitative PCR analysis (qChIP-PCR) was performed with the Power SYBR green PCR Master Mix using the 7300 Real Time PCR system (Applied Biosystems). Oligonucleotides used for qChIP-PCR are listed in Dataset S13.

ChIP-Seq Library Preparation and Illumina Sequencing. ChIP-Seq libraries were constructed starting from 4 ng of ChIP or Input DNA as reported in Blecher-Gonen et al. (71). Libraries were quantified using the KAPA SYBR FAST Universal qPCR Kit (KAPA Biosystems), normalized to 10 nM, pooled, and sequenced with the Illumina HiSEq. 2000 instrument as single-end 100-bp reads.

ChIP-Seq Analysis. Sequencing data were acquired through the default Illumina pipeline using Casava v1.8. Reads were aligned to the human genome (UCSC hg19) using the Bowtie2 aligner v2.1.0 (72), allowing up to two mismatches to cope with human variation. Duplicate reads (i.e., reads of identical-length mapping to exactly the same genomic locations) were removed with SAM tools v0.1.19 using the rmdup option (73). Read counts were normalized to the total number of reads aligned in a library (reads per million). Peak detection was done using the ChIPseeqer v2.0 algorithm (74), enforcing a minimum fold-change of 2 between ChIP and input reads, a minimum peak width of 100 bp, and a minimum distance of 100 bp between peaks. The

threshold for statistical significance of peaks was set at 10^{-5} for NOTCH1, and 10^{-15} for H3K4me1, H3K4me3, and H3K27Ac (Dataset S2). Peaks within 1 kb of centromeric or telomeric regions were removed. H3K4me1 and H3K27Ac peaks were stitched together into regions if located within ±2 kb and ±12.5 kb of each other, respectively, unless they started within a 2-kb window around the TSS. H3K27me3 peaks were called using the RSEG algorithm (75) with 100-bp bin size; only peaks above 5 kb in size were considered.

Motif Enrichment Analysis. Regions within 200 bp of the center of each binding site were searched for motifs from the TRANSFAC 2010 Database. Motifs were represented as position weighted matrices. Using a moving window, motifs were scored against a reference DNA sequence using a log odds ratio comparing the motif's score to a hypothetical score where every base is equally probable. Motifs scoring higher than a given threshold were considered as potentially bound in a location. To determine enrichment in a set of peaks/locations a hypergeometric model was used comparing motifs bound in the peaks to a GC and length controlled set of random genomic sequences.

Definition of Functional Chromatin States of NOTCH1-Bound Genomic Loci. Significant NOTCH1-bound regions occurring at proximal promoters (i.e., within −2/+1 kb from the TSS of an annotated gene) were classified as active if overlapping with H3K4me3, but not H3K27me3, poised if occupied by both H3K4me3 and H3K27me3, and silenced if decorated only by H3K27me3. Distally NOTCH1-bound genomic regions (intergenic or intragenic) were classified as active enhancers if occupied by H3K4me and H3K27Ac, but not H3K4me3, poised if occupied by H3K4me and H3K27me3, and silenced or primed if occupied only by H3K27me3 or H3K4me, respectively. For the identification of superenhancers, we applied the ROSE algorithm (https://bitbucket.org/young_computation/rose) to our H3K27Ac ChIP-Seq datasets (MO1043-ICN1-HA and primary CLL cells). Occupancy of NOTCH1 at superenhancers was then determined based on the overlap between NOTCH1 peaks and genomic regions identified by ROSE. NOTCH1-bound superenhancers were assigned to the nearest expressed and transcriptionally active gene (i.e., distance from superenhancer center to TSS marked by H3K4me3) as the most likely candidate target gene (38).

Primary CLL Cases. Primary CLL cells from the PB of CLL patients ($n = 124$) were obtained from the Feinstein Institute for Medical Research and the Division of Hematology and the Department of Translational Medicine and the Amedeo Avogadro University of Eastern Piedmont. Diagnosis of CLL was based on International Workshop on Chronic Lymphocytic Leukemia-National Cancer Institute Working Group criteria (76) and confirmed by a flow cytometry score >3. The percentage of tumor cells of CLL cases was estimated by cytofluorimetry analysis for $CD5^+/CD19^+$ PB cells of 93 of 124 CLL cases, and it was ≥70% in 90 cases and between 57% and 60% in 3 cases. CLL cases included in the RNA-Seq panel are highlighted in Fig. S2*A*. $ICN1^+$ *NOTCH1*–wild-type cases were selected for RNA-Seq analysis based on a ratio of ICN1 expression > 0.1 compared with the levels observed in the CUTLL1 cell line in the low-exposure immunoblot image. Quantitation of signal intensity was obtained with the ImageJ software (https://imagej.nih.gov/ij/) by subtracting the background signal measured above each band from the signal measured in each band; areas of the same size (set on the image of ICN1 in the CUTLL1 cell line) were used for all measurements. Values were expressed as ratio relative to the CUTLL1 protein sample, set at 1, after normalization for the β-actin loading control. The study was approved by the Institutional Review Board of Columbia University, by the Ethical Committee of the Azienda Ospedaliera Maggiore della Carità di Novara, Amedeo Avogadro University of Eastern Piedmont, and by the Northwell Health's Institutional Review Board and was conducted according to the principles of the World Medical Association Declaration of Helsinki.

DNA Extraction, *IGHV* Mutational Status, and Sanger Sequencing of *NOTCH1*. Genomic DNA was extracted with the QIAamp DNA Mini Kit (Qiagen) and verified for integrity by gel electrophoresis. *IGHV* mutational status was performed as previously described (3, 13). The *NOTCH1* gene portion encoding the PEST domain and the 3′UTR of the *NOTCH1* gene were screened by Sanger targeted sequencing, as previously reported (3, 7).

Gene-Expression Profiling of Human Mature B-Cell Subsets. Raw expression values of GeneChip Human Genome U133 Plus 2.0 (Affymetrix) data from normal mature B-cell subsets were normalized using the Robust Multiarray Averaging algorithm in GenePattern (https://www.broadinstitute.org/cancer/software/genepattern/), and multiple probes corresponding to the same gene were collapsed to a single probe based on the maximum *t*-statistic/maximum SD.

RNA Extraction, cDNA Synthesis, and Quantitative Real-Time PCR. Total RNA was extracted from primary CLL cases with the RNeasy Mini Kit (Qiagen) with on-column DNase treatment. cDNA synthesis was performed using the SuperScript First-Strand Synthesis System (Life Technologies), according to the manufacturer's instructions. The ABsolute QPCR SYBR green mix (Thermo Scientific) was used to amplify specific cDNA fragments with the oligonucleotides listed in Dataset S13, in the 7300 Real-Time PCR system (Applied Biosystems). Data were analyzed by the change-in-threshold ($2^{-\Delta\Delta CT}$) method (77), using GAPDH as a housekeeping reference gene.

RNA-Sequencing of ICN1-HA and Control eGFP MO1043 Cells and Primary CLL Cases. Four MO1043-ICN1-HA and 4 MO1043-eGFP replicates and 49 primary CLL cases were subjected to RNA-Sequencing. Briefly, poly-A pull-down was performed to enrich mRNAs from total RNA samples and libraries were prepared using the Illumina TruSeq RNA prep kit and sequenced using the Illumina HiSeq.2000 instrument at the Columbia Genome Center. MO1043-ICN1-HA and MO1043-eGFP samples were multiplexed to obtain an average of 33,022,292 single-end 100-bp reads per sample; primary CLL samples were multiplexed to obtain an average of 61,266,691 paired-end 100-bp reads per sample (Dataset S3). Real-time analysis (Illumina) was used for base calling and bcl2fastq (v1.8.4) for converting BCL to fastq format, coupled with adaptor trimming. Reads were mapped to the reference genome (Human: NCBI/build37.2) using Tophat (v2.0.4) with 4 mismatches (–read-mismatches = 4) and 10 maximum multiple hits (–max-multihits = 10) (78). The relative abundance of genes was assessed using cufflinks (v2.0.2) with default settings (79). Hierarchical clustering of MO1043-ICN1-HA and -eGFP profiles was performed using the Pearson correlation average linkage, filtering for genes with a minimum $\log_2$-transformed expression value of 5 and a minimum SD of 1. Genes differentially expressed between MO1043-ICN1-HA and -eGFP profiles were determined by an unpaired unequal variance two-tailed Student's *t* test using a FDR ≤ 0.001 (after Benjamini–Hochberg correction) (80). For visualization of gene-expression intensity, expression data were converted to *z*-scores.

GSEA. Gene-expression profile data from mature B cells, MO1043-ICN1-HA and MO1043-eGFP cells, and from primary CLL cases were analyzed for enrichment in NOTCH1-related gene sets with GSEA-2.0 and 1,000 phenotype permutations (27). Enrichments were considered significant with a $P < 0.05$ after correction for multiple hypothesis.

Functional Categories and Pathways Analyses of the NOTCH1-Regulated Genes. Genes directly regulated by NOTCH1 in CLL were assigned to functional categories or annotated pathways using the publicly available bioinformatic tool DAVID 2008 6.7 (Database for Annotation, Visualization and Integrated Discovery, https://david-d.ncifcrf.gov) and the Molecular Signatures Database from the Broad Institute (MSigDBv5.1, CP Geneset, https://www.broadinstitute.org/gsea/msigdb/index.jsp). Only pathways relevant for B-cell biology, based on current knowledge, were selected for further discussion.

Statistical Analyses. Statistical analysis was performed using the GraphPad Prism 5 software (GraphPad Software). The specific test adopted for each analysis is described in each figure legend.

ACKNOWLEDGMENTS. We thank Jon Aster for providing the NOTCH1 antisera used for ChIP-Seq of NOTCH1 in chronic lymphocytic leukemia cells; Ben K. Seon for the MO1043 cell line; Elias Campo and Jennifer Brown for sharing useful information; and the Genomic Technologies Shared Resource for sequencing the ChIP-Seq and the RNA-Seq libraries. This work was supported by the US National Institutes of Health Grant R01-CA177319 (to R.D.-F. and A.A.F.); Special Program Molecular Clinical Oncology 5 × 1000 No. 10007, Associazione Italiana per la Ricerca sul Cancro Foundation Milan, Italy and Progetto Ricerca Finalizzata RF-2011-02349712, Ministero della Salute, Rome, Italy (to G.G.); National Institutes of Health Grant K99/R00 CA197869 and an Alex's Lemonade Stand Foundation Young Investigator grant (to D.H.); and a Leukemia & Lymphoma Society Fellowship (to C.S.).

1. Fabbri G, Dalla-Favera R (2016) The molecular pathogenesis of chronic lymphocytic leukaemia. *Nat Rev Cancer* 16(3):145–162.
2. Pekarsky Y, Zanesi N, Croce CM (2010) Molecular basis of CLL. *Semin Cancer Biol* 20(6):370–376.
3. Fabbri G, et al. (2011) Analysis of the chronic lymphocytic leukemia coding genome: Role of NOTCH1 mutational activation. *J Exp Med* 208(7):1389–1401.
4. Puente XS, et al. (2011) Whole-genome sequencing identifies recurrent mutations in chronic lymphocytic leukaemia. *Nature* 475(7354):101–105.

5. Wang L, et al. (2011) SF3B1 and other novel cancer genes in chronic lymphocytic leukemia. *N Engl J Med* 365(26):2497–2506.
6. Quesada V, et al. (2011) Exome sequencing identifies recurrent mutations of the splicing factor SF3B1 gene in chronic lymphocytic leukemia. *Nat Genet* 44(1):47–52.
7. Puente XS, et al. (2015) Non-coding recurrent mutations in chronic lymphocytic leukaemia. *Nature* 526(7574):519–524.
8. Weng AP, et al. (2004) Activating mutations of NOTCH1 in human T cell acute lymphoblastic leukemia. *Science* 306(5694):269–271.
9. Belver L, Ferrando A (2016) The genetics and mechanisms of T cell acute lymphoblastic leukaemia. *Nat Rev Cancer* 16(8):494–507.
10. Kopan R, Ilagan MX (2009) The canonical Notch signaling pathway: Unfolding the activation mechanism. *Cell* 137(2):216–233.
11. Guruharsha KG, Kankel MW, Artavanis-Tsakonas S (2012) The Notch signalling system: Recent insights into the complexity of a conserved pathway. *Nat Rev Genet* 13(9):654–666.
12. Rossi D, et al. (2012) Mutations of NOTCH1 are an independent predictor of survival in chronic lymphocytic leukemia. *Blood* 119(2):521–529.
13. Fabbri G, et al. (2013) Genetic lesions associated with chronic lymphocytic leukemia transformation to Richter syndrome. *J Exp Med* 210(11):2273–2288.
14. Balatti V, et al. (2012) NOTCH1 mutations in CLL associated with trisomy 12. *Blood* 119(2):329–331.
15. Stilgenbauer S, et al. (2014) Gene mutations and treatment outcome in chronic lymphocytic leukemia: Results from the CLL8 trial. *Blood* 123(21):3247–3254.
16. Pozzo F, et al. (2016) NOTCH1 mutations associate with low CD20 level in chronic lymphocytic leukemia: Evidence for a NOTCH1 mutation-driven epigenetic dysregulation. *Leukemia* 30(1):182–189.
17. Maura F, et al. (2015) Insulin growth factor 1 receptor expression is associated with NOTCH1 mutation, trisomy 12 and aggressive clinical course in chronic lymphocytic leukaemia. *PLoS One* 10(3):e0118801.
18. Arruga F, et al. (2014) Functional impact of NOTCH1 mutations in chronic lymphocytic leukemia. *Leukemia* 28(5):1060–1070.
19. Kluk MJ, et al. (2013) Gauging NOTCH1 activation in cancer using immunohistochemistry. *PLoS One* 8(6):e67306.
20. Onaindia A, et al. (2015) Chronic lymphocytic leukemia cells in lymph nodes show frequent NOTCH1 activation. *Haematologica* 100(5):e200–e203.
21. Stein H, et al. (1980) Immunohistologic analysis of the organization of normal lymphoid tissue and non-Hodgkin's lymphomas. *J Histochem Cytochem* 28(8):746–760.
22. Rosati E, et al. (2009) Constitutively activated Notch signaling is involved in survival and apoptosis resistance of B-CLL cells. *Blood* 113(4):856–865.
23. Klein U, et al. (2003) Transcriptional analysis of the B cell germinal center reaction. *Proc Natl Acad Sci USA* 100(5):2639–2644.
24. Klein U, et al. (2001) Gene expression profiling of B cell chronic lymphocytic leukemia reveals a homogeneous phenotype related to memory B cells. *J Exp Med* 194(11):1625–1638.
25. Seifert M, et al. (2012) Cellular origin and pathophysiology of chronic lymphocytic leukemia. *J Exp Med* 209(12):2183–2198.
26. Kulis M, et al. (2012) Epigenomic analysis detects widespread gene-body DNA hypomethylation in chronic lymphocytic leukemia. *Nat Genet* 44(11):1236–1242.
27. Subramanian A, et al. (2005) Gene set enrichment analysis: A knowledge-based approach for interpreting genome-wide expression profiles. *Proc Natl Acad Sci USA* 102(43):15545–15550.
28. Andersson ER, Lendahl U (2014) Therapeutic modulation of Notch signalling—Are we there yet? *Nat Rev Drug Discov* 13(5):357–378.
29. Kawata A, et al. (1993) Establishment and characterization of the tumors of chronic lymphocytic leukemia cell line in nude and SCID mice. *Leuk Res* 17(10):883–894.
30. Meerbrey KL, et al. (2011) The pINDUCER lentiviral toolkit for inducible RNA interference in vitro and in vivo. *Proc Natl Acad Sci USA* 108(9):3665–3670.
31. Shlyueva D, Stampfel G, Stark A (2014) Transcriptional enhancers: From properties to genome-wide predictions. *Nat Rev Genet* 15(4):272–286.
32. Bernstein BE, et al. (2006) A bivalent chromatin structure marks key developmental genes in embryonic stem cells. *Cell* 125(2):315–326.
33. Béguelin W, et al. (2013) EZH2 is required for germinal center formation and somatic EZH2 mutations promote lymphoid transformation. *Cancer Cell* 23(5):677–692.
34. Pott S, Lieb JD (2015) What are super-enhancers? *Nat Genet* 47(1):8–12.
35. Whyte WA, et al. (2013) Master transcription factors and mediator establish super-enhancers at key cell identity genes. *Cell* 153(2):307–319.
36. Lovén J, et al. (2013) Selective inhibition of tumor oncogenes by disruption of super-enhancers. *Cell* 153(2):320–334.
37. Hnisz D, et al. (2013) Super-enhancers in the control of cell identity and disease. *Cell* 155(4):934–947.
38. Chapuy B, et al. (2013) Discovery and characterization of super-enhancer-associated dependencies in diffuse large B cell lymphoma. *Cancer Cell* 24(6):777–790.
39. Ewen ME, et al. (1993) Functional interactions of the retinoblastoma protein with mammalian D-type cyclins. *Cell* 73(3):487–497.
40. Joshi I, et al. (2009) Notch signaling mediates G1/S cell-cycle progression in T cells via cyclin D3 and its dependent kinases. *Blood* 113(8):1689–1698.
41. Cimmino A, et al. (2005) miR-15 and miR-16 induce apoptosis by targeting BCL2. *Proc Natl Acad Sci USA* 102(39):13944–13949.
42. De Falco F, et al. (2015) Notch signaling sustains the expression of Mcl-1 and the activity of eIF4E to promote cell survival in CLL. *Oncotarget* 6(18):16559–16572.
43. Roberts AW, et al. (2016) Targeting BCL2 with venetoclax in relapsed chronic lymphocytic leukemia. *N Engl J Med* 374(4):311–322.
44. Hayden MS, Ghosh S (2008) Shared principles in NF-kappaB signaling. *Cell* 132(3):344–362.
45. Cornall RJ, et al. (1998) Polygenic autoimmune traits: Lyn, CD22, and SHP-1 are limiting elements of a biochemical pathway regulating BCR signaling and selection. *Immunity* 8(4):497–508.
46. Reth M, Brummer T (2004) Feedback regulation of lymphocyte signalling. *Nat Rev Immunol* 4(4):269–277.
47. Burger JA (2011) Nurture versus nature: The microenvironment in chronic lymphocytic leukemia. *Hematology: ASH Education Program* 2011(1):96–103.
48. Calissano C, et al. (2009) In vivo intraclonal and interclonal kinetic heterogeneity in B-cell chronic lymphocytic leukemia. *Blood* 114(23):4832–4842.
49. Rossi D, et al. (2011) The genetics of Richter syndrome reveals disease heterogeneity and predicts survival after transformation. *Blood* 117(12):3391–3401.
50. Herranz D, et al. (2014) A NOTCH1-driven MYC enhancer promotes T cell development, transformation and acute lymphoblastic leukemia. *Nat Med* 20(10):1130–1137.
51. Palomero T, et al. (2006) NOTCH1 directly regulates c-MYC and activates a feed-forward-loop transcriptional network promoting leukemic cell growth. *Proc Natl Acad Sci USA* 103(48):18261–18266.
52. Ryan RJ, et al. (2015) Detection of enhancer-associated rearrangements reveals mechanisms of oncogene dysregulation in B-cell lymphoma. *Cancer Discov* 5(10):1058–1071.
53. Edelmann J, et al. (2012) High-resolution genomic profiling of chronic lymphocytic leukemia reveals new recurrent genomic alterations. *Blood* 120(24):4783–4794.
54. Holmes R, Zuniga-Pflucker JC (2009) The OP9-DL1 system: Generation of T-lymphocytes from embryonic or hematopoietic stem cells in vitro. *Cold Spring Harb Protoc* 2009(2):pdb.prot5156.
55. O'Neil J, et al. (2007) FBW7 mutations in leukemic cells mediate NOTCH pathway activation and resistance to gamma-secretase inhibitors. *J Exp Med* 204(8):1813–1824.
56. Messmer BT, et al. (2005) In vivo measurements document the dynamic cellular kinetics of chronic lymphocytic leukemia B cells. *J Clin Invest* 115(3):755–764.
57. Gómez-del Arco P, et al. (2010) Alternative promoter usage at the Notch1 locus supports ligand-independent signaling in T cell development and leukemogenesis. *Immunity* 33(5):685–698.
58. Ashworth TD, et al. (2010) Deletion-based mechanisms of Notch1 activation in T-ALL: Key roles for RAG recombinase and a conserved internal translational start site in Notch1. *Blood* 116(25):5455–5464.
59. Haydu JE, et al. (2012) An activating intragenic deletion in NOTCH1 in human T-ALL. *Blood* 119(22):5211–5214.
60. Guy CS, et al. (2013) Distinct TCR signaling pathways drive proliferation and cytokine production in T cells. *Nat Immunol* 14(3):262–270.
61. Fortini ME, Bilder D (2009) Endocytic regulation of Notch signaling. *Curr Opin Genet Dev* 19(4):323–328.
62. Zhao B, et al. (2011) Epstein-Barr virus exploits intrinsic B-lymphocyte transcription programs to achieve immortal cell growth. *Proc Natl Acad Sci USA* 108(36):14902–14907.
63. Zhang X, et al. (2016) Identification of focally amplified lineage-specific super-enhancers in human epithelial cancers. *Nat Genet* 48(2):176–182.
64. Shi J, et al. (2013) Role of SWI/SNF in acute leukemia maintenance and enhancer-mediated Myc regulation. *Genes Dev* 27(24):2648–2662.
65. Rossi D, et al. (2013) Integrated mutational and cytogenetic analysis identifies new prognostic subgroups in chronic lymphocytic leukemia. *Blood* 121(8):1403–1412.
66. Wu Y, et al. (2010) Therapeutic antibody targeting of individual Notch receptors. *Nature* 464(7291):1052–1057.
67. Bereshchenko OR, Gu W, Dalla-Favera R (2002) Acetylation inactivates the transcriptional repressor BCL6. *Nat Genet* 32(4):606–613.
68. Pasqualucci L, Kitaura Y, Gu H, Dalla-Favera R (2006) PKA-mediated phosphorylation regulates the function of activation-induced deaminase (AID) in B cells. *Proc Natl Acad Sci USA* 103(2):395–400.
69. Dominguez-Sola D, et al. (2012) The proto-oncogene MYC is required for selection in the germinal center and cyclic reentry. *Nat Immunol* 13(11):1083–1091.
70. Wang H, et al. (2011) Genome-wide analysis reveals conserved and divergent features of Notch1/RBPJ binding in human and murine T-lymphoblastic leukemia cells. *Proc Natl Acad Sci USA* 108(36):14908–14913.
71. Blecher-Gonen R, et al. (2013) High-throughput chromatin immunoprecipitation for genome-wide mapping of in vivo protein-DNA interactions and epigenomic states. *Nat Protoc* 8(3):539–554.
72. Langmead B, Salzberg SL (2012) Fast gapped-read alignment with Bowtie 2. *Nat Methods* 9(4):357–359.
73. Li H, et al.; 1000 Genome Project Data Processing Subgroup (2009) The Sequence Alignment/Map format and SAMtools. *Bioinformatics* 25(16):2078–2079.
74. Giannopoulou EG, Elemento O (2011) An integrated ChIP-seq analysis platform with customizable workflows. *BMC Bioinformatics* 12:277.
75. Song Q, Smith AD (2011) Identifying dispersed epigenomic domains from ChIP-Seq data. *Bioinformatics* 27(6):870–871.
76. Hallek M, et al.; International Workshop on Chronic Lymphocytic Leukemia (2008) Guidelines for the diagnosis and treatment of chronic lymphocytic leukemia: A report from the International Workshop on Chronic Lymphocytic Leukemia updating the National Cancer Institute-Working Group 1996 guidelines. *Blood* 111(12):5446–5456.
77. Livak KJ, Schmittgen TD (2001) Analysis of relative gene expression data using real-time quantitative PCR and the 2(-Delta Delta C(T)) method. *Methods* 25(4):402–408.
78. Trapnell C, Pachter L, Salzberg SL (2009) TopHat: Discovering splice junctions with RNA-Seq. *Bioinformatics* 25(9):1105–1111.
79. Trapnell C, et al. (2010) Transcript assembly and quantification by RNA-Seq reveals unannotated transcripts and isoform switching during cell differentiation. *Nat Biotechnol* 28(5):511–515.
80. Benjamini YH (1995) Controlling the false discovery rate—A practical and powerful approach to multiple testing. *J R Stat Soc Series B Stat Methodol* 57:289–300.
81. Basso K, Dalla-Favera R (2015) Germinal centres and B cell lymphomagenesis. *Nat Rev Immunol* 15(3):172–184.
82. Victora GD, et al. (2012) Identification of human germinal center light and dark zone cells and their relationship to human B-cell lymphomas. *Blood* 120(11):2240–2248.
83. Palomero T, et al. (2006) CUTLL1, a novel human T-cell lymphoma cell line with t(7;9) rearrangement, aberrant NOTCH1 activation and high sensitivity to gamma-secretase inhibitors. *Leukemia* 20(7):1279–1287.
84. Khan A, Zhang X (2016) dbSUPER: A database of super-enhancers in mouse and human genome. *Nucleic Acids Res* 44(D1):D164–D171.